Constraining the uncertainty associated with sea salt aerosol parameterizations in global models using nudged UKESM1-AMIP simulations

Abhijith Ulayottil Venugopal[1], Yusuf A. Bhatti[2], Olaf Morgenstern[3], Jonny Williams[4], Nicholas John Edkins[3], Catherine Hardacre[1], Anthony Crawford Jones[5], and Laura Revell[1]

[1]University of Canterbury
[2]SRON Netherlands Institute for Space Research
[3]NIWA
[4]University of Reading
[5]University of Exeter

May 28, 2024

Abstract

Sea salt is the largest source of natural aerosol in the atmosphere by mass. Formed when ocean waves break and bubbles burst, sea salt aerosols (SSA) influence Earth's climate via direct and indirect processes. Models participating in the sixth Coupled Model Intercomparison project (CMIP6) demonstrate a negative effective radiative forcing when SSA emissions are doubled. However, the magnitude of the effective radiative forcing ranges widely from -0.35 +/- 0.04 W/mˆ2 to -2.28 +/- 0.07 W/mˆ2, with the largest difference over the Southern Ocean. Differences in the response to doubled SSA emissions arise from model uncertainty (e.g. individual model physics, aerosol size distribution) and parameterization uncertainty (e.g. how SSA is produced in the model). Here, we perform single-model experiments with UKESM1-AMIP incorporating all of the SSA parameterizations used by the current generation of CMIP6 Earth system models. Using a fixed SSA size distribution, our experiments show that the parameterization uncertainty causes large inter-model diversity in SSA emissions in the models, particularly over the tropics and the Southern Ocean. The choice of parameterization influences the ambient aerosol size distribution, cloud condensation nuclei and cloud droplet number concentrations, and therefore direct and indirect radiative forcing. We recommend that modelling groups evaluate their SSA parameterizations and update them where necessary in preparation for future model intercomparison activities

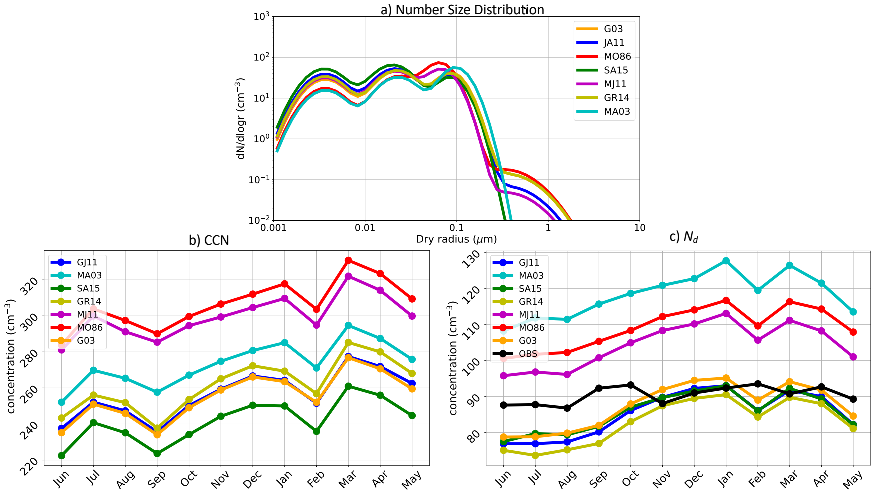
a) Number Size Distribution
dN/dlogr (cm⁻³)
Dry radius (μm)
G03
JA11
MO86
SA15
MJ11
GR14
MA03
b) CCN
concentration (cm⁻³)
GJ11
MA03
SA15
GR14
MJ11
MO86
G03
c) N_d
OBS
Jun
Jul
Aug
Sep
Oct
Nov
Dec
Jan
Feb
Mar
Apr
May

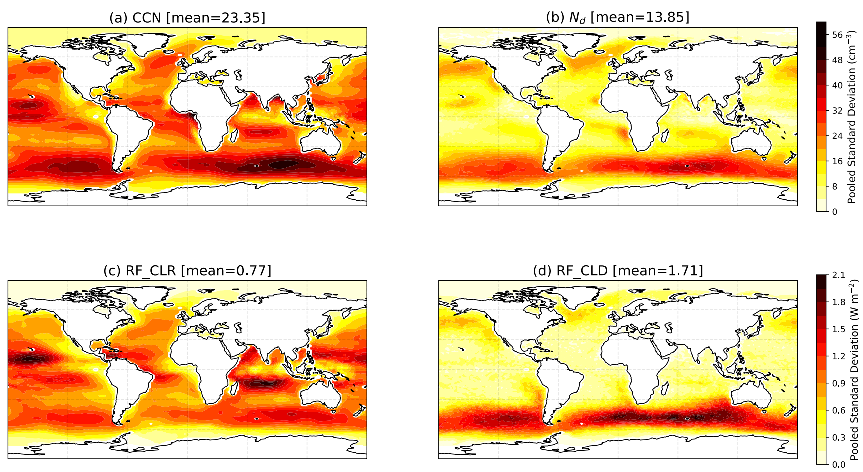
(a) CCN [mean=23.35]
(b) N_d [mean=13.85]
Pooled Standard Deviation (cm⁻³)
(c) RF_CLR [mean=0.77]
(d) RF_CLD [mean=1.71]
Pooled Standard Deviation (W m⁻²)

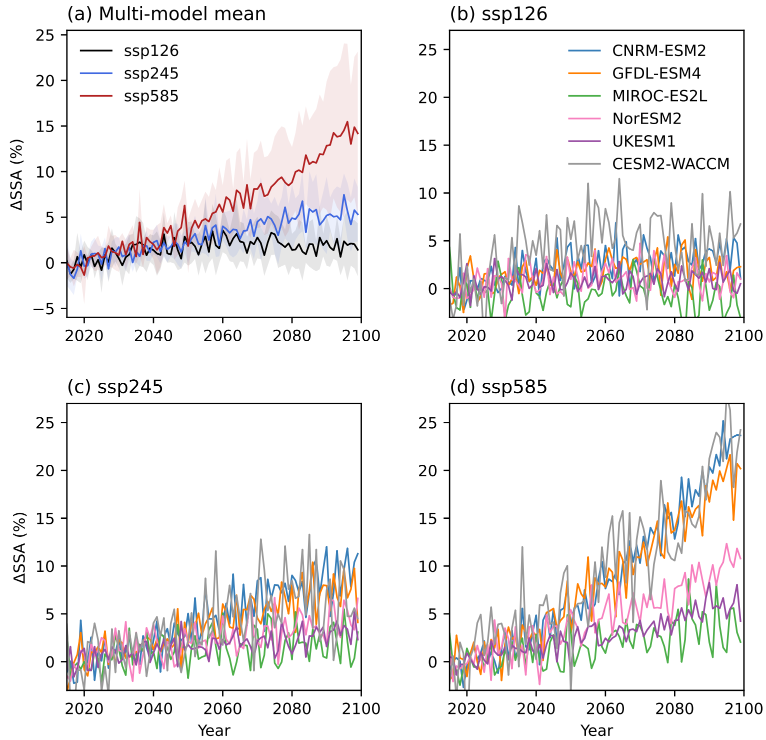
(a) Multi-model mean
(b) ssp126
(c) ssp245
(d) ssp585
ssp126
ssp245
ssp585
CNRM-ESM2
GFDL-ESM4
MIROC-ES2L
NorESM2
UKESM1
CESM2-WACCM
ΔSSA (%)
Year

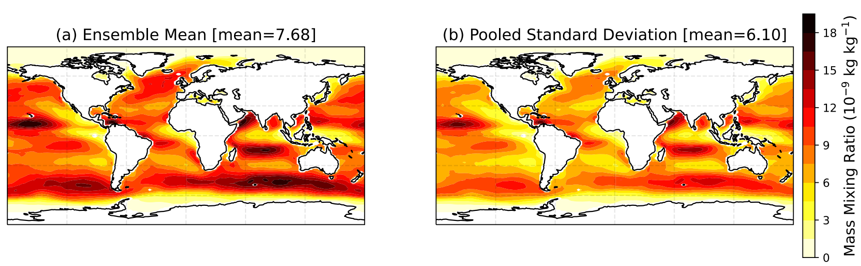
(a) Ensemble Mean [mean=7.68]
(b) Pooled Standard Deviation [mean=6.10]
Mass Mixing Ratio (10^{-9} kg kg^{-1})

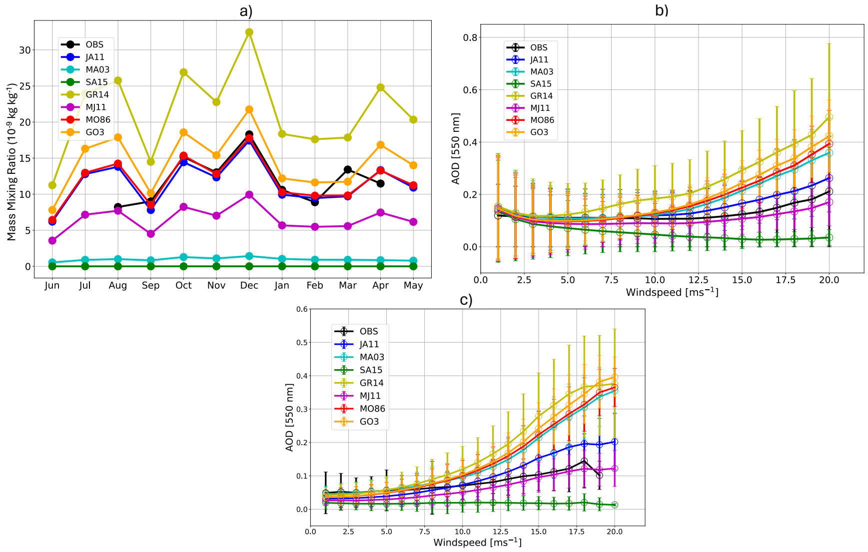
a)
b)
c)
OBS
JA11
MA03
SA15
GR14
MJ11
MO86
GO3
Mass Mixing Ratio (10^{-9} kg kg^{-1})
AOD [550 nm]
Windspeed [ms^{-1}]
Jun
Jul
Aug
Sep
Oct
Nov
Dec
Jan
Feb
Mar
Apr
May

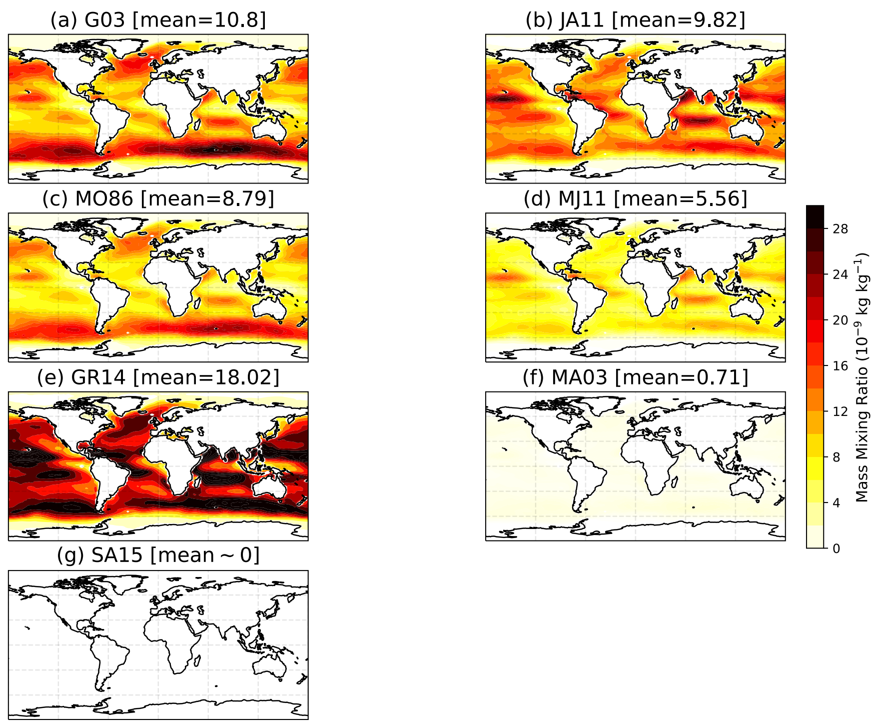
(a) G03 [mean=10.8]
(b) JA11 [mean=9.82]
(c) MO86 [mean=8.79]
(d) MJ11 [mean=5.56]
(e) GR14 [mean=18.02]
(f) MA03 [mean=0.71]
(g) SA15 [mean ~ 0]
Mass Mixing Ratio (10^{-9} kg kg^{-1})

Constraining the uncertainty associated with sea salt aerosol parameterizations in global models using nudged UKESM1-AMIP simulations

Abhijith U. Venugopal[1], Yusuf A. Bhatti[1,#], Olaf Morgenstern[2], Jonny Williams[2,&], Nick Edkins[1,2], Catherine Hardacre[1], Anthony Jones[3], Laura E. Revell[1]

[1]School of Physical and Chemical Sciences, University of Canterbury, Christchurch, New Zealand
[2]National Institute of Water and Atmospheric Research, Wellington, New Zealand
[3]Met Office, Exeter, United Kingdom
[#]Now at SRON Netherlands Institute for Space Research, Leiden, the Netherlands
[&]Now at Reading University, Department of Meteorology, UK

Key Points:

- Parameterization uncertainty is critical in driving inter-model differences in global sea salt aerosol (SSA) emissions
- Uncertainties in SSA emissions cascade to uncertainties in cloud and aerosol radiative forcing, especially over the Southern Ocean
- The default SSA parameterization in UKESM1 overestimates SSA emissions, but other parameterizations give better agreement with observations

Corresponding author: Abhijith U.Venugopal, `abhijith.ulayottilvenugopal@canterbury.ac.nz`

Corresponding author: Laura E. Revell, `laura.revell@canterbury.ac.nz`

Abstract

Sea salt is the largest source of natural aerosol in the atmosphere by mass. Formed when ocean waves break and bubbles burst, sea salt aerosols (SSA) influence Earth's climate via direct and indirect processes. Models participating in the sixth Coupled Model Intercomparison project (CMIP6) demonstrate a negative effective radiative forcing when SSA emissions are doubled. However, the magnitude of the effective radiative forcing ranges widely from -0.35 $\pm$ 0.04 W m^{-2} to -2.28 $\pm$ 0.07 W m^{-2}, with the largest difference over the Southern Ocean. Differences in the response to doubled SSA emissions arise from model uncertainty (e.g. individual model physics, aerosol size distribution) and parameterization uncertainty (e.g. how SSA is produced in the model). Here, we perform single-model experiments with UKESM1-AMIP incorporating all of the SSA parameterizations used by the current generation of CMIP6 Earth system models. Using a fixed SSA size distribution, our experiments show that the parameterization uncertainty causes large inter-model diversity in SSA emissions in the models, particularly over the tropics and the Southern Ocean. The choice of parameterization influences the ambient aerosol size distribution, cloud condensation nuclei and cloud droplet number concentrations, and therefore direct and indirect radiative forcing. We recommend that modelling groups evaluate their SSA parameterizations and update them where necessary in preparation for future model intercomparison activities.

Plain Language Summary

Sea salt aerosols (SSA) are the main source of natural aerosols in the Earth's atmosphere and are formed when waves break and bubbles burst at the ocean surface. SSA are important for Earth's climate as they reduce the amount of sunlight reaching the surface by predominantly scattering light and seeding cloud formation. Therefore, SSA production is routinely included in Earth system models. Different models represent SSA production differently—some base it on the wind speed close to the ocean's surface, while others include additional factors such as the sea surface temperature. Combined with differences in modelled meteorology, this means that Earth system models all produce different amounts of SSA at different locations. To date, no one has examined how the way sea salt aerosols are produced in the current generation of Earth system models cascades to other important processes in the climate system such as cloud formation. Here we use one model to test seven different representations of SSA. We show that the uncertainties associated with SSA production are large and that modelling groups should pay careful attention to the way their model produces sea salt aerosol for future model intercomparison efforts.

1 Introduction

Sea salt aerosols (SSA) are formed when waves break and bubbles burst at the ocean surface. Droplets of sea salt, combined with marine organic matter, are injected into the atmosphere as film, jet and spume droplets (Grythe et al., 2014). SSA influences the climate system directly, by scattering sunlight, and indirectly, by seeding cloud formation which subsequently affects cloud lifetime and reflectivity, along with subsequent impacts on precipitation (Twomey, 1977; Murphy et al., 1998).

Together with dust, SSA is a leading contributor of aerosol mass to the atmosphere (Grythe et al., 2014). However, there is low confidence in how SSA emissions may change in the future due to uncertainties in formation pathways and their response to increasing greenhouse gas concentrations (Szopa et al., 2021). Thornhill et al. (2021) evaluated the effective radiative forcing (ERF) from a doubling of SSA emissions in Earth system models (ESMs) participating in the sixth Climate Model Intercomparison Project (CMIP6, Eyring et al. (2016)). All of the models produced a negative ERF, indicating agreement that an increase in SSA leads to climate cooling. However, the magnitude of the ERF varied widely, ranging between -0.35 ± 0.04 W m^{-2} to -2.28 ± 0.07 W m^{-2} (Thornhill et al., 2021). In addition, our analysis of SSA projections in the 21st century in CMIP6 models show a divergent response, particularly under the high greenhouse gas emissions scenario Shared Socioeconomic Pathways (SSP) 5-8.5 (Figure 1). Models that include SST in their SSA parameterization such as GFDL-ESM4, CNRM-ESM2 and CESM2-WACCM show a ≈20–25% increase in global-mean SSA production through the 21st century, while those that rely on wind speed alone show smaller increases of ≈3–5% (e.g. UKESM1).

SSA production is affected by wind speed, wave state, sea surface temperature (SST), salinity, viscosity, sea ice cover and the presence of organic material in seawater (Grythe et al., 2014; Song et al., 2023). Parameterizations of SSA production in ESMs are typically based on near-surface wind speed, which influences wave state (S. Gong, 2003; Monahan & Mac Niocaill, 1986). Some parameterizations additionally include a SST term to ameliorate underestimated aerosol optical depth (AOD) in the tropics (Jaeglé et al., 2011; Salter et al., 2015; Grythe et al., 2014; Mårtensson et al., 2003). The parameterizations are typically based on whitecap methods (which assume that the area of the ocean covered with whitecaps is indicative of SSA production) and empirical fits to observations, or laboratory studies (Monahan & Mac Niocaill, 1986; S. Gong, 2003; Salter et al., 2015; Grythe et al., 2014).

The ESMs participating in CMIP6 use various parameterizations to represent SSA production (Lapere et al., 2023), which could explain the large variation in ERF when SSA emissions were doubled (Thornhill et al., 2021) and the divergent projections shown under SSP5-8.5 in Figure 1. Other differences could arise from how winds, SST and sea ice cover are represented, as these factors influence SSA production (Song et al., 2023). Or, differences could arise from the assumed aerosol size distribution and maximum particle cut-off diameters (Lapere et al., 2023). In an investigation of the performance of CMIP6 models in simulating SSA emissions in polar regions, Lapere et al. (2023) performed offline calculations to predict SSA mass fluxes. They showed that for a constant wind speed, SST and maximum particle size, the choice of SSA flux parameterization induced a large uncertainty in the SSA mass flux ranging over an order of magnitude or more.

Here, we performed ESM simulations with specified dynamics (nudging) to investigate uncertainties resulting from the choice of SSA parameterization. We tested seven SSA parameterizations, all used by present-day Earth system models (Section 2) in the atmosphere-only configuration of the United Kingdom Earth System Model (UKESM1-AMIP; Sellar et al. (2019)). We then examined how SSA parameterization uncertainty cascades to uncertainty in SSA emission, cloud microphysics and radiative forcing. The novelty of our approach lies in the use of a single ESM with fixed meteorology and consistent SSA treatment (e.g. SSA density, optical properties, size distribution) and handling of aerosol-cloud interactions. This allows the sensitivity of ERF to the choice of SSA emissions parameterization to be elucidated, which cannot be done via CMIP6-type model intercomparison projects.

2 Methods

2.1 Model description

Simulations were performed using UKESM1-AMIP (Sellar et al., 2019). UKESM1-AMIP has a horizontal grid resolution of 1.25° × 1.875°. The atmosphere contains 85 unevenly spaced levels extending to 85 km above the surface. Aerosol evolution, growth and deposition are handled by the Global Model of Aerosol Processes (GLOMAP; Mulcahy et al. (2020)). GLOMAP is a two-moment modal aerosol microphysics scheme which simulates the mass and number concentration of sea salt, $SO_4{}^{2-}$, black carbon and organic aerosol (Mulcahy et al., 2020). Mineral dust is represented separately using a bin emission scheme (Woodward, 2001). GLOMAP simulates aerosol species across five log-normal size modes: a soluble nucleation mode with geometric mean dry radius 0.5–5 nm, a soluble and insoluble Aitken mode, both spanning 5–50 nm, a soluble accumulation mode (50–250 nm) and a soluble coarse mode (250–5000 nm). By default, SSA fluxes are parameterized using the formulation of S. Gong (2003) (Table 1 and Table 2) and SSA is mapped into the accumulation and coarse modes (maximum cut-off size–5000 nm). SSA is assumed to originate only from the ocean surface; SSA from blowing snow is not represented (e.g. X. Gong et al. (2023)).

2.2 Simulation description

Simulations were run for a period of 18 months, from December 2004 to May 2006. The first six months were discarded as spin-up and we focus our analysis on the 12 months spanning June 2005 to May 2006. Wind speed (u, v) and temperature were nudged to 6-hourly reanalysis data as described by Telford et al. (2008). Fifth generation ECMWF (ERA-5) reanalysis data were used for nudging (Hersbach et al., 2020). Nudging was applied to ensure that wind speeds, which drive SSA production, were consistently represented across all simulations. While nudging to temperature can produce less accurate simulations of clouds and precipitation (Sun et al., 2019), we applied it here to ensure that the simulations were as consistent as possible with each other. SST and sea ice concentrations were prescribed from Hadley Centre Global Sea Ice and Sea Surface Temperature data (Titchner & Rayner, 2014).

2.3 Sensitivity simulations

Seven simulations were performed, each using one of the SSA parameterizations shown in Tables 1 and 2. While numerous parameterizations for SSA production exist (Grythe et al., 2014), these seven were selected because they are used by ESMs participating in CMIP6 (Thornhill et al., 2021). The parameterizations typically assume that the flux of SSA has a power law dependence on the near-surface (10 m) wind speed. For the parameterizations of S. Gong (2003) (hereafter 'G03') and Monahan and Mac Niocaill (1986) ('MO86'), wind speed is the only driver of SSA production. The parameterizations of Salter et al. (2015) ('SA15'), Jaeglé et al. (2011) ('JA11'), Grythe et al. (2014) ('GR14') and Mårtensson et al. (2003) ('MA03') also include SST. The JA11 parameterization was developed to reconcile biases between models and observations in the tropics, where wind speeds are typically low and the surface ocean is warm (Jaeglé et al., 2011). It has since been incorporated alongside other parameterizations, such as MO86 to be used in the GFDL-ESM4 model (Table 1 and Table 2). Although the JA11 parameterization wasn't used by any of the CMIP6 models, we include it here as it has been found to compare favourably with observations (Revell et al., 2021).

For each simulation we examined the SSA mass mixing ratio, 550 nm AOD, cloud condensation nuclei (CCN) concentration, cloud droplet number concentration (N_d) and changes in radiative forcing (ΔRF). Here ΔRF is defined as the difference in the top-of-atmosphere net radiation relative to the G03 simulation, which represents the default SSA parameterization in UKESM1. As discussed earlier, the size range remains fixed in all the simulations (0–5000 nm in terms of particle dry radius). The SSA emitted in each of the parameterizations are mapped only into the accumulation and coarse modes and the separation depends on whether the particle radius is below or above of the upper-limit of accumulation mode in UKESM1-AMIP (250 nm).

Table 1: SSA parameterizations implemented in UKESM1-AMIP sensitivity simulations. Details of the parameterizations are given in Table 2.

CMIP6 model	SSA parameterization	SSA driver(s)
UKESM1	S. Gong (2003) [G03]	wind speed
MIROC-ES2L, GISS	Monahan and Mac Niocaill (1986) [MO86]	wind speed
GFDL-ESM4	Monahan and Mac Niocaill (1986) & Jaeglé et al. (2011) [MJ11]	wind speed, SST
NorESM2	Salter et al. (2015) [SA15]	wind speed, SST
CNRM-ESM2	Grythe et al. (2014) [GR14]	wind speed, SST
CESM2-WACCM	Mårtensson et al. (2003) [MA03]	wind speed, SST
This study	S. Gong (2003) & Jaeglé et al. (2011) [JA11]	wind speed, SST

Table 2: SSA parameterizations

	SSA parameterization
[a] G03	$1.373u_{10}^{3.41}r^{-A}(1+0.057r^{3.45}10^{1.607e^{-B^2}})$
MO86	$1.373u_{10}^{3.41}r^{-3}(1+0.057r^{1.05}10^{1.19e^{-B^2}})$
[b]MJ11	$(0.3+0.1SST-0.0076SST^2+0.00021SST^3)\ (1.373u_{10}^{3.41}r^{-3}(1+0.057r^{1.05}10^{1.19e^{-B^2}})$
[c*]SA15	$F_{ent_{(u10)}}(A_i.SST^3+B_i.SST^2+C_i.SST+D_i)$
[d]GR14	$(0.3+0.1SST-0.0076SST^2+0.00021SST^3)\ (235u_{10}^{3.5}\exp(-0.55[\ln(D_p/0.1)]^2)$ $+(0.2u_{10}^{3.5}\exp(-1.5[\ln(D_p/3)]^2)\ +(6.8u_{10}^{3}\exp(-1[\ln(D_p/30)]^2)$
[e*]MA03	$(A_k.SST+B_k).W$, for $D_p\leq 2.8\ \mu m$ $D_p\geq 2.8\ \mu m$,$1.373u_{10}^{3.41}r^{-3}(1+0.057r^{1.05}10^{1.19e^{-B^2}})$
JA11	$(0.3+0.1SST-0.0076SST^2+0.00021SST^3)\ 1.373u_{10}^{3.41}r^{-A}(1+0.057r^{3.45}10^{1.607e^{-B^2}})$

[a] r is the particle radius at 80% relative humidity. u_{10} is the windspeed at the height of 10 m
$A = 4.7(1+\theta r)^{-0.017r^{-1.44}}$ and $B = 0.433 - log(r)0.433$, where θ is the an adjustable parameter to control the SSA size distribution.
[b] SST is sea-surface temperature.
[c] $F_{ent_{(u10)}}$ is the volume of air entrained as per unit area per unit time as a function of u_{10} and is given by: $F_{ent_{(u10)}} = 2(\pm 1)10^{-8}u_{10}^{3.41}$
A, B and C are polynomial coefficients for the number flux of each of the three modes.
[d] D_p is the dry particle diameter.
[e] W is the white cap area and is given by: $3.84\times 10^{-4}u_{10}^{3.41}$
A_k and B_k are co-efficients of parameterization dependent on the size interval.
[*] Further details on the co-efficients are given in Table S1 and Table S2

2.4 Observations

Simulated AOD is compared to daily AOD retrieved from Moderate Resolution Imaging Spectroradiometer (MODIS)-Aqua measurements at 550 nm (Sayer et al., 2014). Aqua measurements are available from 2002 and we choose the data for the year 2005 to compare with the simulations. We also note that the period between 2003-2007 was volcanically quiescent, making the contribution of volcanic aerosol towards the total aerosol burden insignificant. Datasets used here are retrieved from combined deep blue (land retrieval only) and dark target (combined land and ocean) algorithms and have a spatial resolution of $1^\circ \times 1^\circ$. Simulated N_d is also compared with N_d retrieved from MODIS measurements (Grosvenor et al., 2018). Land regions were masked during the analysis for both the AOD and N_d datasets. SSA data from the Southern Ocean are limited, especially in terms of long-running time series. We compared simulated SSA mixing ratios to measurements made at the Cape Grim Baseline Air Pollution Station at Kennaook/Cape Grim (40.38°S, 144.4°E) Australia, which is one of the few data sets available in the Southern Ocean region spanning more than a few months.

3 Results and discussion

3.1 Impact of SSA parameterizations on sea salt aerosol concentrations

Figure 2 shows annual-mean SSA mixing ratios in the sensitivity simulations with the different SSA parameterizations described in Table 1. The mean SSA mass mixing ratio exhibits higher values over the Southern Ocean and in the tropics, most likely facilitated by favourable physical conditions such as higher wind speeds and SSTs, respectively (Figure 2a; Grythe et al. (2014); Liu et al. (2021); Jaeglé et al. (2011). Furthermore, the largest variability is seen in these same regions (Figure 2b). Overall, we find that the global average pooled standard deviation (6.10×10^{-9} kg kg^{-1}) is around 80% of the ensemble mean (7.60×10^{-9} kg kg^{-1}). Because our simulations all use the same nudged UKESM1-AMIP configuration, we can attribute the large standard deviation in SSA mass mixing ratio to the SSA parameterizations rather than differences in model physics such the aerosol scheme (bin vs. modal), maximum cut-off diameter, or meteorological factors that influence SSA emission such as wind speed, SST and sea ice cover.

To gain an understanding of which simulations, if any, compare well to observations, we compared SSA mass mixing ratios to measurements from the Cape Grim Baseline Air Pollution Station at Kennaook/Cape Grim (40.38°S, 144.4°E) Australia (Figure 3a). In addition to the data availability during the simulation period, this station was chosen due to its proximity to the Southern Ocean where some of the highest SSA concentrations and highest variability are found due to the dominance of south-westerly flow at the site (Jiang et al., 2021; Heintzenberg et al., 2000). Observed SSA mass mixing ratios vary between ≈ 10–15×10^{-9} kg kg^{-1}, whereas there is substantially larger variability across the UKESM1-AMIP simulations with different parameterizations (≈ 0–30×10^{-9} kg kg^{-1}). The parameterizations that give the best agreement with the observations are JA11 and MO86 (Figure 3a). In contrast, the model under-predicts SSA mass mixing ratio to the greatest extent with SA15 and MA03, while it over-predicts SSA mass mixing ratio to the greatest extent with GR14. As discussed by Grythe et al. (2014), GR14 has a higher windspeed dependency in its parameterization compared to the rest (e.g. $u^{3.5}$ in GR14 vs. $u^{3.45}$ in G03) which is likely contributing to higher SSA production. We attribute under-prediction of SSA mass mixing ratios in the SA15 simulation to the application of the source function to specific modal diameters (0.95, 0.6 and 1.5 µm) unlike most other parameterizations that addresses the whole the size distribution

(Table 2 and Table S1). In addition, Salter et al. (2015) also notes uncertainty in wind-speed dependency in the parameterization ($u^{3.41}$ vs. $u^{3.74}$). These factors may have contributed to the parameterization of SA15 not effectively simulating SSA emission when implemented within UKESM1. Similarly, the parameterization of MA03 involves a combination of parameterizations (e.g. $(A_kSST+B_k)W$ for diameter < 2.5 µm and MO86 for diameter $>$ 2.5 µm) (Table 2) and usage of different co-efficients for different size ranges within the parameterization of $(A_kSST+B_k)W$ (Table S1). W in the parameterization represents the white cap area and A_k and B_k are the co-efficients dependent on the size interval. SSA emissions from the MA03 parameterization implemented in UKESM1 are minimal, and occur predominantly in the accumulation mode (section 3.1).

AOD is the integral of the extinction co-efficient of aerosols in a column air and reflects the total aerosol content within that column. In the marine atmosphere sulfate aerosol, dust and SSA contribute to AOD; the dominant contributor is SSA(Quinn & Bates, 2014; Bates et al., 2006). The global mean AOD diverges across the UKESM1-AMIP simulations above wind speeds of 6 m s^{-1}(Figure 3b). At wind speeds of 20 m s^{-1} simulated AOD varies between 0.01 $\pm$ 0.005 and 0.4 $\pm$ 0.05 (Figure 3b). As the wind speed increases above $\approx$ 6 m s^{-1} AOD also increases in most of the simulations. It is known that most of the wave breaking processes and consequent bubble generation occurs when the wind speed exceeds $\approx$ 5 m s^{-1}(Grythe et al., 2014). The increase in AOD beyond this wind speed threshold of $\approx$ 6 m s^{-1} reflects accelerated SSA generation. However, the simulations using the JA11, MO86, MA03, G03 and GR14 parameterizations have a higher sensitivity to wind speed than indicated by observations and over-predict AOD above the threshold of 6 m s^{-1} both globally and during the austral winter (June, July, August; JJA) (Figure 3b-c). This was also reported by Revell et al. (2019), who found the G03 parameterization implemented in HadGEM3-GA7.1, a predecessor of UKESM1-AMIP, overestimated wintertime AOD over the Southern Ocean at high wind speeds. This reflects the over-dependence of SSA emissions on wind speed in these parameterizations (Revell et al., 2019). On the other hand, the SA15 parameterization under-predicts AOD to the greatest extent globally, and over the Southern Ocean, and is unable to represent increasing AOD above wind speeds of 6 m s^{-1}. This is due to SA15 having too low SSA emissions as discussed above. Figures 3b–c show that the observed AOD is best captured by the UKESM-AMIP simulations with the JA11 and MJ11 parameterizations, which are the parameterizations of G03 and MO86 scaled with a SST factor proposed by Jaeglé et al. (2011).

While the parameterizations of G03 and MO86 are only wind speed dependent, the parameterizations of JA11, MA03, SA15, GR14 and MJ11 also have SST influencing SSA production. SSA production increases with increasing SST in the JA11, GR14 and MA03 parameterizations, but decreases with increasing SST in the SA15 parameterization (Salter et al., 2015; Lapere et al., 2023). Observations suggest that the overall production of SSA increases with increasing SST (Liu et al., 2021). However, laboratory experiments produce complex and inconclusive results (Song et al., 2023; Grythe et al., 2014). Christiansen et al. (2019) show that the concentration of SSA produced can change with changes to the instrumental set-up as it would result in different rates of air entrainment. They showed that when using a diffuser to generate air bubbles, SSA concentrations decreased linearly when temperature increased from -2 °C to 35 °C, which approximately encompasses the global ocean temperature range. Using a plunging jet resulted in reduced production of SSA with increasing temperature until 10 °C and an increase thereafter. A previous study by Salter et al. (2015) also showed a non-linear decrease in the SSA concentration for the temperature range between -1 °C to 30 °C. Our results show that understanding the precise effect of SST on SSA emissions is vital to reducing aerosol uncertainty associated with parameterizations.

In the following sections, we assess how each of the SSA parameterizations affects the aerosol number size distribution, cloud microphysics and finally the impact on radiative forcing.

3.2 Aerosol size distribution and cloud microphysics

Figure 4a shows the global-mean aerosol number size distribution for UKESM1-AMIP sensitivity simulations. The size distribution provides information on how aerosol number concentrations are distributed across various size modes (in UKESM1 these are the nucleation, Aitken, accumulation and coarse modes, see Section 2). The nucleation mode is characterized by the formation of new particles by the condensation of gas-phase species on their own (homogeneous nucleation) or in the presence of pre-existing particles (heterogeneous nucleation) (Chin & Kahn, 2009). These newly-formed particles can coagulate (forming the Aitken mode) and when the particles grow further either through condensation of vapours onto their surface or coagulation, the accumulation mode forms (Chin & Kahn, 2009). The coarse mode is associated with mechanical processes such as bubble bursting to form SSA, and emission of other primary particles, such as dust (Chin & Kahn, 2009). In UKESM1, sea-salt is emitted in to both the accumulation and coarse modes.

As shown in Figure 4a, the coarse mode is not present in the simulations using the SA15 and MA03 parameterizations. While all the other parameterizations consist of a single SSA source function across the entire size range considered (0.005 µm–5 µm in radius), the parameterization of SA15 and MA03 contain different source functions or different co-efficients for particles with different diameters in the source function(Salter et al., 2015; Mårtensson et al., 2003). This appears to affect the aerosol partitioning into the different modes in the simulations using these parameterizations. In the case of the accumulation mode, we note that the simulations that used the MO86, MJ11 and MA03 parameterizations (Figure 3a) had higher accumulation mode aerosol number concentrations. Because aerosols >0.05 µm are likely to be activated as CCN (Rose et al., 2017) (which corresponds to the accumulation and coarse modes in UKESM1), this indicates that the choice of SSA parameterization can influence cloud formation.

To better understand the impact of various SSA parameterizations on cloud microphysical properties, we now examine the concentration of CCN and N_d (Figure 4a and b). CCN is an indicator for the potential to form cloud droplets at the top of the cloud (approximately 800 m), whereas N_d is the actual number of droplets formed at the cloud base. The parameterizations of MO86, MJ11 and MA03 show higher concentrations of CCN in comparison to other parameterizations (on average between 270 cm^{-3} and 310 cm^{-3}; Figure 4c), with MO86 exhibiting the highest concentrations. Examining N_d, it is interesting to note that the parameterization of MA03 shows the highest concentration, followed by MO86 and MJ11. N_d is driven by factors such as cloud updraft velocity, wind shear, supersaturation, and CCN concentration (Rosenfeld et al., 2019). In turn, CCN concentrations are affected by the size distribution. The simulation using the MA03 parameterization contains larger accumulation mode particles compared to the simulations that use MO86 and MJ11 (Figure 4a). Hence, MA03 has more potential to form cloud droplets. As the simulations are nudged and the meteorology is consistent across all the simulations, it is likely that this difference in size distribution is the reason for the higher N_d values in the simulation with the MA03 parameterization. The remaining parameterizations of G03, GR14, JA11 and SA15 produce similar concentrations of N_d. Comparison with the MODIS N_d (Grosvenor et al., 2018) indicates that these four parameterizations are closer to the observations, at least between November - May, but that all the parameterizations are unable to capture N_d from June until October. The calculation of N_d is based on optical depth and effective radius from MODIS measurements and assumes that (i) the concentration of the droplet in the cloud is constant vertically and (ii) the liquid water content of the cloud increases linearly with cloud height

(Grosvenor et al., 2018). Both assumptions are not applicable to all types of clouds and are mostly valid only for stratocumulous clouds (Grosvenor et al., 2018). In addition, MODIS N_d is known to be more uncertain over the regions with less cloud cover, such as ocean regions. Thus, it is necessary to be cautious in validating N_d from simulations with MODIS N_d.

We also examined spatial variability in CCN and N_d to understand which regions are most sensitive to SSA parameterization. Figure 5a shows that simulated CCN was most variable over the Southern Ocean, followed by the tropics, mirroring the changes seen in the SSA mixing ratio (Figure 2b). Interestingly, N_d, unlike CCN, was only variable over the Southern Ocean. The under-estimation of N_d over the Southern Ocean is a long-standing problem in climate and Earth system models (McCoy et al., 2020). McCoy et al. (2020) suggest that this underestimation of N_d could be a result of too little and too inefficient CCN production. The sensitivity of N_d towards SSA parameterizations in our analysis indicates that improved representation of SSA emission can also be important for addressing the model bias in N_d over the Southern Ocean. This is consistent with the findings from Revell et al. (2019). The reduced variability observed in N_d over the tropics could be from oversaturation in N_d as droplets are formed both from both natural and anthropogenic emissions, and/or from a strong sink due to elevated humidity, temperature and tropical convection.

3.3 Impact of SSA parameterizations on radiative forcing

Given that the choice of SSA parameterization affects the aerosol number size distribution, CCN concentration and N_d concentration (Figure 4b), we expect radiative forcing (RF) to be affected too. We calculated the difference in all-sky, clear-sky and cloudy-sky radiative forcing relative to the G03 simulation (ΔRF), which represents the default parameterization in UKESM1-AMIP. A positive ΔRF indicates relative warming compared to the G03 simulation due to an increase in incoming (solar) radiation or a decrease in outgoing (terrestrial) radiation, and vice-versa for a negative ΔRF. We find that the Southern Ocean region has large variability in CCN, N_d, clear-sky RF and cloudy-sky RF, while the tropics have large variability in CCN and clear-sky RF (Figure 5), matching the regions where there is large variability in SSA mass mixing ratios (see Figure 2). Thus, we infer that the choice of parameterization can influence direct and indirect SSA radiative effects and may contribute to the inter-model diversity in radiative forcing in CMIP6 models, as noted by Thornhill et al. (2021).

Table 3 shows the all-sky, clear-sky and cloudy sky ΔRF for each SSA parameterization. We find that the net all-sky ΔRF varies from +2.69 W m^{-2} (SA15 minus G03) to -2.66 W m^{-2} (MA03 minus G03), demonstrating that changing the SSA parameterization in UKESM1-AMIP can have an overall warming or cooling impact relative to the default G03 parameterization. In general, positive clear-sky ΔRF values were associated with low SSA mass mixing ratios and therefore low AOD, for example when the SA15 and MJ11 parameterizations are implemented in UKESM1-AMIP. As the aerosol burden is lower, more radiation is able to reach the surface, thus leading to warming. In contrast, the negative clear-sky ΔRF values occurred when AOD was relatively high (see the GR14 parameterization in Figure 3b), causing incoming solar radiation to be reflected and scattered to a greater extent than in G03. In the case of GR14, this is due to high SSA mass mixing ratios.

Positive cloudy-sky ΔRF is associated with reduced SSA in the accumulation mode and therefore lower CCN and N_d compared with UKESM1-AMIP-G03. This occurred with the JA11, SA15 and GR14 parameterizations. Generally, the reduction in cloud cover increases the solar radiation reaching the surface causing the surface to warm. In the UKESM1-AMIP simulations where cloudy-sky ΔRF are negative, such as MO86, MJ11 and MA04,

Table 3: Change in the global- annual-mean radiative forcing (ΔRF) with respect to the default UKESM1-AMIP SSA parameterization, G03.

Difference	All-sky	Clear-sky	Cloudy-sky
JA11-G03	0.43 (2.16%)	0.04 (0.56%)	0.38 (1.41%)
MO86-G03	-2.24 (-11.24%)	-0.03 (-0.42%)	-2.21 (-8.05%)
MJ11-G03	-1.41 (-7.08%)	0.61 (8.14%)	-2.02 (-7.37%)
SA15-G03	2.69 (13.47%)	1.49 (19.85%)	1.19 (4.35%)
GR14-G03	-0.30 (-1.50%)	-1.06 (-14.21%)	0.76 (2.79%)
MA03-G03	-2.66 (-13.39%)	0.16 (2.11%)	-2.83 (-10.30%)

SSA in the accumulation mode increased relative to G03, resulting in higher CCN and N_d values.

The largest all-sky ΔRF values, positive or negative, occurred when the clear-sky and cloudy ΔRF values were additive/complementing. For example, in the SA15 simulation, the combination of low AOD, and CCN and N_d concentrations compared with G03, had a substantial warming impact (ΔRF = +2.69 W m^{-2}, see Table 3), while the high AOD, CCN and N_d in the MA03 simulation had a substantial cooling impact (ΔRF = -2.66 W m^{-2}, see Table 3). In contrast, opposing signs for the clear-sky and cloudy-sky ΔRF reduced the overall impact on ΔRF, such as in the simulations that used the MJ11 and GR14 parameterizations. In the case of GR14, despite having higher SSA mass mixing ratio, and thus AOD, compared to G03, the distribution of SSA, particularly in the accumulation mode is not very different to G03, thus minimizing the impact of higher clear-sky RF. Whereas in MJ11, the opposite happens: the pronounced cooling effect from higher cloudy-sky RF is reduced by the warming from lower clear-sky RF, as the emission of SSA is lower in MJ11 when compared to G03. In summary we find that the combined changes in AOD and cloud microphysics, and their consequent impacts on clear-sky and cloudy-sky ΔRF, is important to the overall impact on all-sky ΔRF.

3.4 Optimal SSA parameterization for UKESM1-AMIP

Revell et al. (2019) have shown that, compared to observations, the G03 parameterization for SSA in UKESM1 overestimates SSA production over the Southern Ocean, in agreement with our findings (Figure 3b). Comparison with observations of SSA from a region of maximum varibility (Cape Grim/Southern Ocean) and with AOD over the global ocean (a potential index for SSA concentration globally) show that the JA11 and MJ11 parameterizations are best able to capture SSA mass mixing ratios and AOD (Figure 3b). Further, JA11 does not alter the aerosol size distribution or cloud microphysics such that the radiative forcing is substantially changed compared to G03. In contrast, the MJ11 parameterization, which combines MO86 and JA11 (Section 3.2), exacerbates the overprediction of N_d in UKESM1-AMIP because MO86 over-produces SSA for the size < 0.2 µm (S. Gong, 2003). For this reason the MO86 parameterization was replaced by G03 in UKESM1 (S. Gong, 2003; Mulcahy et al., 2020).

While we remain mindful of the unresolved impact of SST on SSA emissions we suggest that the JA11 parameterization improves the simulation of SSA in UKESM1-AMIP and will help to improve the model's representation of aerosol over the Southern

Ocean. In the context of on-going and future warming, a parameterization with an SST component is likely to be better positioned to reflect changes in SSA emission, initiate and respond to climate feedbacks, and drive better understanding of the climate impacts. We also note that the magnitude and the uncertainty in the simulated variables (SSA mass mixing ratio, AOD, CCN, N_d) in UKESM1-AMIP simulations are not absolute and are likely to differ when implemented in other models. This also means the parameterizations that didn't simulate SSA well in UKESM1 (e.g SA15), may perform better when used in their 'native' models.

4 Summary and Outlook

In this study, we implemented seven different SSA parameterizations that have been used in CMIP6 models into UKESM1-AMIP. In performing simulations with these SSA parameterizations using a uniform model set-up, we have quantified inter-model variability in radiative forcing due to SSA emission parameterization.

The choice of SSA parameterization influenced both clear-sky and cloud-sky radiative forcing over the Southern Ocean, while tropical regions were only sensitive to clear-sky radiative changes as the changes in N_d were minimal over the tropics. This may be due to oversaturation in N_d in the tropics as droplets are formed from both natural and anthropogenic emissions in this region, and/or because there is a strong sink due to elevated humidity, temperature and tropical convection. Our analysis illustrates the cascading effects of SSA mass mixing ratio on aerosol number size distribution, CCN concentration, N_d and ultimately radiative forcing. We find that the choice of parameterization influences radiative forcing directly, by driving how much SSA is emitted, and indirectly by affecting the aerosol size distribution. Importantly, it is the balance between the amount of SSA emitted and how much is partitioned to the accumulation mode that controls the overall impact on RF. Our study also shows that the G03 SSA parameterization currently used in UKESM1 overproduces sea-salt and we recommend combining it with the SST source function of Jaeglé et al. (2011).

Because SSA is a large source of natural aerosol over the Southern Ocean, constraining the uncertainty associated with SSA emission parameterization in climate and Earth system models is extremely important for constraining uncertainty in aerosol radiative forcing and more confidently predicting how our climate will change in the future. This is particularly true in the Southern Ocean where SSA is the dominant aerosol component and where aerosol-climate interactions are highly uncertain, (McCoy et al., 2020; Revell et al., 2019, 2021), limiting our ability to understand how this vast region will respond to and drive climate change.

5 Open Research

MODIS AOD data were accessed via the Giovanni online data system, developed and maintained by the NASA GES DISC (`https://giovanni.gsfc.nasa.gov`). N_d data were obtained from the Centre for Environmental Data Analysis(`https://data.ceda.ac.uk/badc/deposited2018/Grosvenor/_modis/_droplet/_conc`). ERA-5 data were obtained from the European Centre for Medium-Range Weather Forecasts (`https://cds.climate.copernicus.eu`). CMIP6 data were accessed through Earth System Grid Federation (ESGF) repository (`https://esgf-node.llnl.gov`), and via Danabasoglu (2019a), Seferian (2018), Seland et al. (2019a), Hajima et al. (2019), Tang et al. (2019), Krasting et al. (2018), John et al. (2018), Seland et al. (2019b), Tachiiri et al. (2019), Good et al. (2019), Danabasoglu (2019b), and Voldoire (2019).

Acknowledgments

We acknowledge the Deep South National Science Challenge (C01X1901) for their support of this research and the UK MetOffice for the use of the MetUM. We wish to acknowledge the contribution of New Zealand eScience Infrastructure (NeSI) high-performance computing facilities to the results of this research. New Zealand's national facilities are provided by NeSI and funded jointly by NeSI's collaborator institutions and through the Ministry of Business, Innovation and Employment's Research Infrastructure program (`https://www.nesi.org.nz`). The authors acknowledge the World Climate Research Programme, which, through its Working Group on Coupled Modeling, coordinated and promoted the sixth Coupled Model Intercomparison Project (CMIP6). We thank the climate modeling groups for producing and making available their model output, the Earth System Grid Federation (ESGF) for archiving the data and providing access, and the multiple funding agencies who support CMIP6 and ESGF. LER appreciates support by the Rutherford Discovery Fellowships from New Zealand Government funding, administered by the Royal Society Te Apārangi. We acknowledge the Cape Grim Science Program for the provision of SSA data from Cape Grim. The Cape Grim Science Program is a collaboration between the Australian Bureau of Meteorology and CSIRO Australia.

References

Bates, T., Anderson, T., Baynard, T., Bond, T., Boucher, O., Carmichael, G., ... others (2006). Aerosol direct radiative effects over the northwest atlantic, northwest pacific, and north indian oceans: estimates based on in-situ chemical and optical measurements and chemical transport modeling. *Atmospheric Chemistry and Physics*, *6*(6), 1657–1732.

Chin, M., & Kahn, R. (2009). *Atmospheric aerosol properties and climate impacts* (Vol. 2). US Climate Change Science Program.

Christiansen, S., Salter, M. E., Gorokhova, E., Nguyen, Q. T., & Bilde, M. (2019). Sea spray aerosol formation: Laboratory results on the role of air entrainment, water temperature, and phytoplankton biomass. *Environmental science & technology*, *53*(22), 13107–13116.

Danabasoglu, G. (2019a). *Ncar cesm2-waccm model output prepared for cmip6 cmip historical.* Earth System Grid Federation. Retrieved from `https://doi.org/10.22033/ESGF/CMIP6.10071` doi: 10.22033/ESGF/CMIP6.10071

Danabasoglu, G. (2019b). *Ncar cesm2-waccm model output prepared for cmip6 scenariomip.* Earth System Grid Federation. Retrieved from `https://doi.org/10.22033/ESGF/CMIP6.10026` doi: 10.22033/ESGF/CMIP6.10026

Eyring, V., Bony, S., Meehl, G. A., Senior, C. A., Stevens, B., Stouffer, R. J., & Taylor, K. E. (2016). Overview of the coupled model intercomparison project phase 6 (cmip6) experimental design and organization. *Geoscientific Model Development*, *9*(5), 1937–1958.

Gong, S. (2003). A parameterization of sea-salt aerosol source function for sub-and super-micron particles. *Global biogeochemical cycles*, *17*(4).

Gong, X., Zhang, J., Croft, B., Yang, X., Frey, M. M., Bergner, N., ... others (2023). Arctic warming by abundant fine sea salt aerosols from blowing snow. *Nature Geoscience*, *16*(9), 768–774.

Good, P., Sellar, A., Tang, Y., Rumbold, S., Ellis, R., Kelley, D., ... Walton, J. (2019). *Mohc ukesm1.0-ll model output prepared for cmip6 scenariomip.* Earth System Grid Federation. Retrieved from `https://doi.org/10.22033/ESGF/CMIP6.1567` doi: 10.22033/ESGF/CMIP6.1567

Grosvenor, D. P., Sourdeval, O., Zuidema, P., Ackerman, A., Alexandrov, M. D., Bennartz, R., ... others (2018). Remote sensing of droplet number concentration in warm clouds: A review of the current state of knowledge and perspectives. *Reviews of Geophysics*, *56*(2), 409–453.

Grythe, H., Ström, J., Krejci, R., Quinn, P., & Stohl, A. (2014). A review of sea-spray aerosol source functions using a large global set of sea salt aerosol concentration measurements. *Atmospheric Chemistry and Physics*, *14*(3), 1277–1297.

Hajima, T., Abe, M., Arakawa, O., Suzuki, T., Komuro, Y., Ogura, T., ... Tachiiri, K. (2019). *Miroc miroc-es2l model output prepared for cmip6 cmip historical.* Earth System Grid Federation. Retrieved from `https://doi.org/10.22033/ESGF/CMIP6.5602` doi: 10.22033/ESGF/CMIP6.5602

Heintzenberg, J., Covert, D., & van Dingenen, R. (2000). Size distribution and chemical composition of marine aerosols: a compilation and review.

Hersbach, H., Bell, B., Berrisford, P., Hirahara, S., Horányi, A., Muñoz-Sabater, J., ... others (2020). The era5 global reanalysis. *Quarterly Journal of the Royal Meteorological Society*, *146*(730), 1999–2049.

Jaeglé, L., Quinn, P., Bates, T., Alexander, B., & Lin, J.-T. (2011). Global distribution of sea salt aerosols: new constraints from in situ and remote sensing observations. *Atmospheric Chemistry and Physics*, *11*(7), 3137–3157.

Jiang, B., Xie, Z., Lam, P. K., He, P., Yue, F., Wang, L., ... Wu, X. (2021). Spatial and temporal distribution of sea salt aerosol mass concentrations in the marine boundary layer from the arctic to the antarctic. *Journal of Geophysical Research: Atmospheres*, *126*(6), e2020JD033892.

John, J. G., Blanton, C., McHugh, C., Radhakrishnan, A., Rand, K., Vahlenkamp, H., ... Zeng, Y. (2018). *Noaa-gfdl gfdl-esm4 model output prepared for cmip6 scenariomip.* Earth System Grid Federation. Retrieved from `https://doi.org/10.22033/ESGF/CMIP6.1414` doi: 10.22033/ESGF/CMIP6.1414

Krasting, J. P., John, J. G., Blanton, C., McHugh, C., Nikonov, S., Radhakrishnan, A., ... Zhao, M. (2018). *Noaa-gfdl gfdl-esm4 model output prepared for cmip6 cmip historical.* Earth System Grid Federation. Retrieved from `https://doi.org/10.22033/ESGF/CMIP6.8597` doi: 10.22033/ESGF/CMIP6.8597

Lapere, R., Thomas, J. L., Marelle, L., Ekman, A. M., Frey, M. M., Lund, M. T., ... others (2023). The representation of sea salt aerosols and their role in polar climate within cmip6. *Journal of Geophysical Research: Atmospheres*, *128*(6), e2022JD038235.

Liu, S., Liu, C.-C., Froyd, K. D., Schill, G. P., Murphy, D. M., Bui, T. P., ... others (2021). Sea spray aerosol concentration modulated by sea surface temperature. *Proceedings of the National Academy of Sciences*, *118*(9), e2020583118.

Mårtensson, E., Nilsson, E., de Leeuw, G., Cohen, L., & Hansson, H.-C. (2003). Laboratory simulations and parameterization of the primary marine aerosol production. *Journal of Geophysical Research: Atmospheres*, *108*(D9).

McCoy, I. L., McCoy, D. T., Wood, R., Regayre, L., Watson-Parris, D., Grosvenor, D. P., ... others (2020). The hemispheric contrast in cloud microphysical properties constrains aerosol forcing. *Proceedings of the National Academy of Sciences*, *117*(32), 18998–19006.

Monahan, E. C., & Mac Niocaill, G. (1986). *Oceanic whitecaps: And their role in air-sea exchange processes* (No. 2). Springer Science & Business Media.

Mulcahy, J. P., Johnson, C., Jones, C. G., Povey, A. C., Scott, C. E., Sellar, A., ... others (2020). Description and evaluation of aerosol in ukesm1 and hadgem3-gc3. 1 cmip6 historical simulations. *Geoscientific Model Development Discussions*, *2020*, 1–59.

Murphy, D., Anderson, J., Quinn, P., McInnes, L., Brechtel, F., Kreidenweis, S., ... Buseck, P. (1998). Influence of sea-salt on aerosol radiative properties in the southern ocean marine boundary layer. *Nature*, *392*(6671), 62–65.

Quinn, P., & Bates, T. (2014). Ocean-derived aerosol and its climate impacts.

Revell, L., Kremser, S., Hartery, S., Harvey, M., Mulcahy, J. P., Williams, J., ... others (2019). The sensitivity of southern ocean aerosols and cloud microphysics to sea spray and sulfate aerosol production in the hadgem3-ga7. 1 chemistry–climate model. *Atmospheric Chemistry and Physics*, *19*(24), 15447–

15466.

Revell, L., Wotherspoon, N., Jones, O., Bhatti, Y., Williams, J., Mackie, S., & Mulcahy, J. (2021). Atmosphere-ocean feedback from wind-driven sea spray aerosol production. *Geophysical Research Letters*, *48*(7), e2020GL091900.

Rose, C., Sellegri, K., Moreno, I., Velarde, F., Ramonet, M., Weinhold, K., ... others (2017). Ccn production by new particle formation in the free troposphere. *Atmospheric Chemistry and Physics*, *17*(2), 1529–1541.

Rosenfeld, D., Zhu, Y., Wang, M., Zheng, Y., Goren, T., & Yu, S. (2019). Aerosol-driven droplet concentrations dominate coverage and water of oceanic low-level clouds. *Science*, *363*(6427), eaav0566.

Salter, M. E., Zieger, P., Acosta Navarro, J. C., Grythe, H., Kirkevåg, A., Rosati, B., ... Nilsson, E. D. (2015). An empirically derived inorganic sea spray source function incorporating sea surface temperature. *Atmospheric Chemistry and Physics*, *15*(19), 11047–11066.

Sayer, A., Munchak, L., Hsu, N., Levy, R., Bettenhausen, C., & Jeong, M.-J. (2014). Modis collection 6 aerosol products: Comparison between aqua's e-deep blue, dark target, and "merged" data sets, and usage recommendations. *Journal of Geophysical Research: Atmospheres*, *119*(24), 13–965.

Seferian, R. (2018). *Cnrm-cerfacs cnrm-esm2-1 model output prepared for cmip6 cmip historical.* Earth System Grid Federation. Retrieved from `https://doi.org/10.22033/ESGF/CMIP6.4068` doi: 10.22033/ESGF/CMIP6.4068

Seland, y., Bentsen, M., Oliviè, D. J. L., Toniazzo, T., Gjermundsen, A., Graff, L. S., ... Schulz, M. (2019a). *Ncc noresm2-lm model output prepared for cmip6 cmip.* Earth System Grid Federation. Retrieved from `https://doi.org/10.22033/ESGF/CMIP6.502` doi: 10.22033/ESGF/CMIP6.502

Seland, y., Bentsen, M., Oliviè, D. J. L., Toniazzo, T., Gjermundsen, A., Graff, L. S., ... Schulz, M. (2019b). *Ncc noresm2-lm model output prepared for cmip6 scenariomip ssp585.* Earth System Grid Federation. Retrieved from `https://doi.org/10.22033/ESGF/CMIP6.8319` doi: 10.22033/ESGF/CMIP6.8319

Sellar, A. A., Jones, C. G., Mulcahy, J. P., Tang, Y., Yool, A., Wiltshire, A., ... others (2019). Ukesm1: Description and evaluation of the uk earth system model. *Journal of Advances in Modeling Earth Systems*, *11*(12), 4513–4558.

Song, A., Li, J., Tsona, N. T., & Du, L. (2023). Parameterizations for sea spray aerosol production flux. *Applied Geochemistry*, 105776.

Sun, J., Zhang, K., Wan, H., Ma, P.-L., Tang, Q., & Zhang, S. (2019). Impact of nudging strategy on the climate representativeness and hindcast skill of constrained eamv1 simulations [Journal Article]. *Journal of Advances in Modeling Earth Systems*, *11*(12), 3911-3933. doi: https://doi.org/10.1029/2019MS001831

Szopa, S., Naik, V., Adhikary, B., Artaxo, P., Berntsen, T., Collins, W., ... others (2021). Short-lived climate forcers. In *Agu fall meeting abstracts* (Vol. 2021, pp. U13B–06).

Tachiiri, K., Abe, M., Hajima, T., Arakawa, O., Suzuki, T., Komuro, Y., ... Kawamiya, M. (2019). *Miroc miroc-es2l model output prepared for cmip6 scenariomip.* Earth System Grid Federation. Retrieved from `https://doi.org/10.22033/ESGF/CMIP6.936` doi: 10.22033/ESGF/CMIP6.936

Tang, Y., Rumbold, S., Ellis, R., Kelley, D., Mulcahy, J., Sellar, A., ... Jones, C. (2019). *Mohc ukesm1.0-ll model output prepared for cmip6 cmip historical.* Earth System Grid Federation. Retrieved from `https://doi.org/10.22033/ESGF/CMIP6.6113` doi: 10.22033/ESGF/CMIP6.6113

Telford, P., Braesicke, P., Morgenstern, O., & Pyle, J. (2008). Description and assessment of a nudged version of the new dynamics unified model. *Atmospheric Chemistry and Physics*, *8*(6), 1701–1712.

Thornhill, G., Collins, W., Olivié, D., Skeie, R. B., Archibald, A., Bauer, S., ... others (2021). Climate-driven chemistry and aerosol feedbacks in cmip6 earth system models. *Atmospheric Chemistry and Physics*, *21*(2), 1105–1126.

Titchner, H. A., & Rayner, N. A. (2014). The met office hadley centre sea ice and sea surface temperature data set, version 2: 1. sea ice concentrations. *Journal of Geophysical Research: Atmospheres*, *119*(6), 2864–2889.

Twomey, S. (1977). The influence of pollution on the shortwave albedo of clouds. *J. atmos. Sci*, *34*, 1149–1152.

Voldoire, A. (2019). *Cnrm-cerfacs cnrm-esm2-1 model output prepared for cmip6 scenariomip ssp585.* Earth System Grid Federation. Retrieved from `https://doi.org/10.22033/ESGF/CMIP6.4226` doi: 10.22033/ESGF/CMIP6.4226

Woodward, S. (2001). Modeling the atmospheric life cycle and radiative impact of mineral dust in the hadley centre climate model. *Journal of Geophysical Research: Atmospheres*, *106*(D16), 18155–18166.

Supplementary Information

Table S1: Co-efficients and size interval for the parameterization of SA15.

Modal diameter (µm)	Ai	B_i	C_i	D_i
0.095	-5.2168×10^5	3.31725×10^8	-6.95275×10^8	1.0684×10^{10}
0.6	0	7.37×10^5	-2.4803×10^7	7.7373×10^8
1.5	0	1.4210×10^4	1.4662×10^7	1.7075×10^8

Table S2: Co-efficients for the parameterization MA03 for three size intervals.

D_p (µm)	c_4	c_3	c_2	c_1	c_0
0.02-0.145	-2.576×10^{35}	5.932×10^{28}	-2.867×10^{21}	-3.003×10^{13}	-2.881×10^{6}
0.145-0.419	-2.452×10^{33}	-2.404×10^{27}	-8.148×10^{20}	1.183×10^{14}	-6.743×10^{6}
0.419-2.8	1.085×10^{29}	-9.841×10^{23}	3.132×10^{18}	-4.165×10^{12}	2.181×10^{6}
Size interval (µm)	d_4	d_3	d_2	d_1	d_0
0.02-0.145	7.188×10^{37}	-1.616×10^{31}	6.791×10^{23}	1.829×10^{16}	7.609×10^{8}
0.145-0.419	7.368×10^{35}	-7.310×10^{29}	2.528×10^{23}	-3.787×10^{16}	2.279×10^{9}
0.419-2.8	-2.859×10^{31}	2.601×10^{26}	-8.297×10^{20}	1.105×10^{15}	-5.800×10^{8}

$*A_k = c_4 - c_0$ and $B_k = d_4 - d_0$

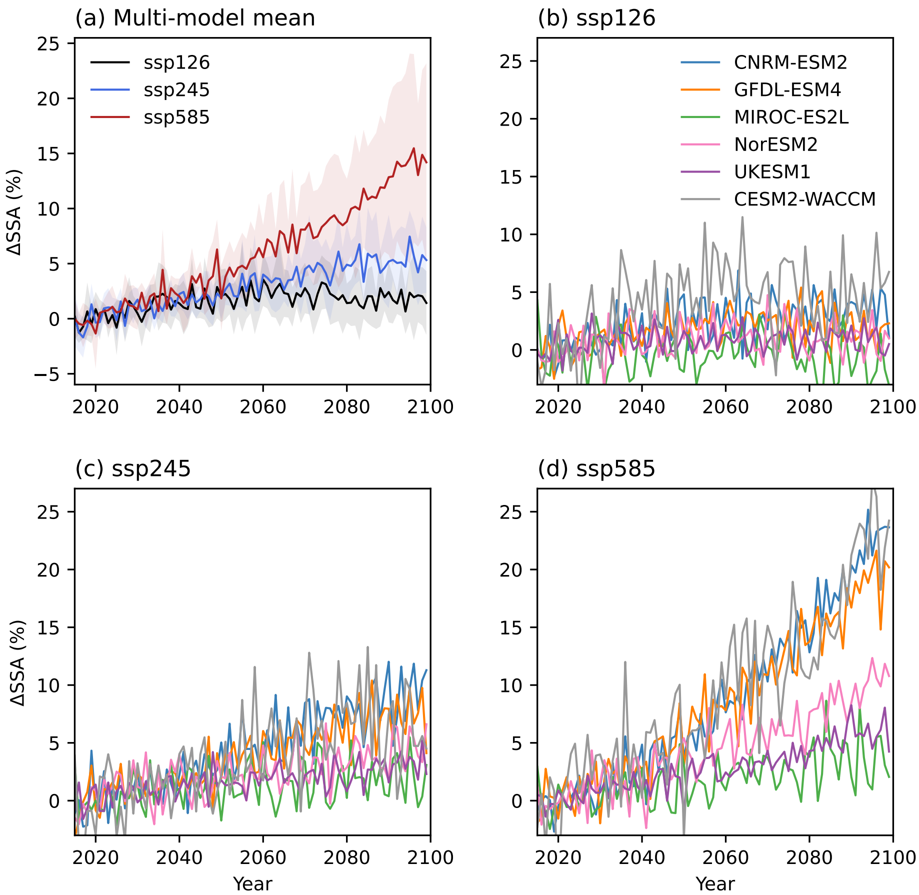

Figure 1: Change in global mean near-surface SSA mass mixing ratio relative to the 2015-2014 average under the Shared Socioeconomic Pathways (SSP) in CMIP6 Earth system models (quantified for this study): GFDL-ESM4 (John et al., 2018), NorESM2 (Seland et al., 2019b), MIROC-ES2L (Tachiiri et al., 2019), CNRM-ESM2 (Voldoire, 2019), CESM2-WACCM (Danabasoglu, 2019b) and UKESM1 (Good et al., 2019). a) Global means, b) SSP1-2.6 (low emission), c) SSP2-4.5 (medium emission), d) SSP5-8.5 (high emission).

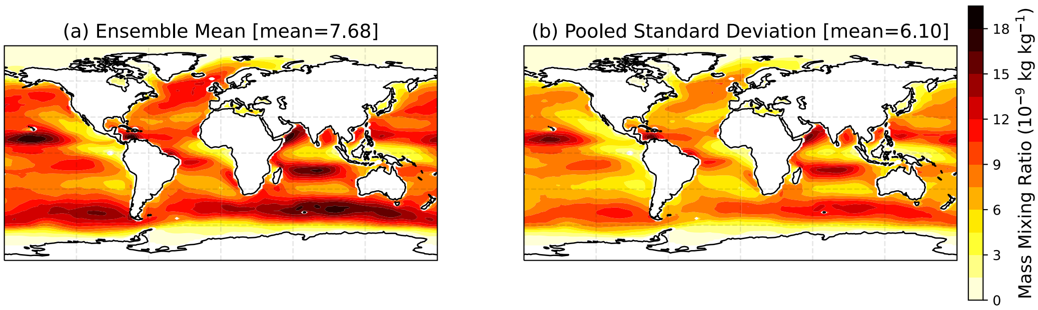

Figure 2: Near-surface annual-mean SSA mass mixing ratios in seven UKESM1-AMIP sensitivity simulations using the SSA parameterizations described in Table 1. (a) Ensemble mean; (b) Pooled standard deviation. The values in the titles indicate global average quantities in 10^{-9} kg kg^{-1}.

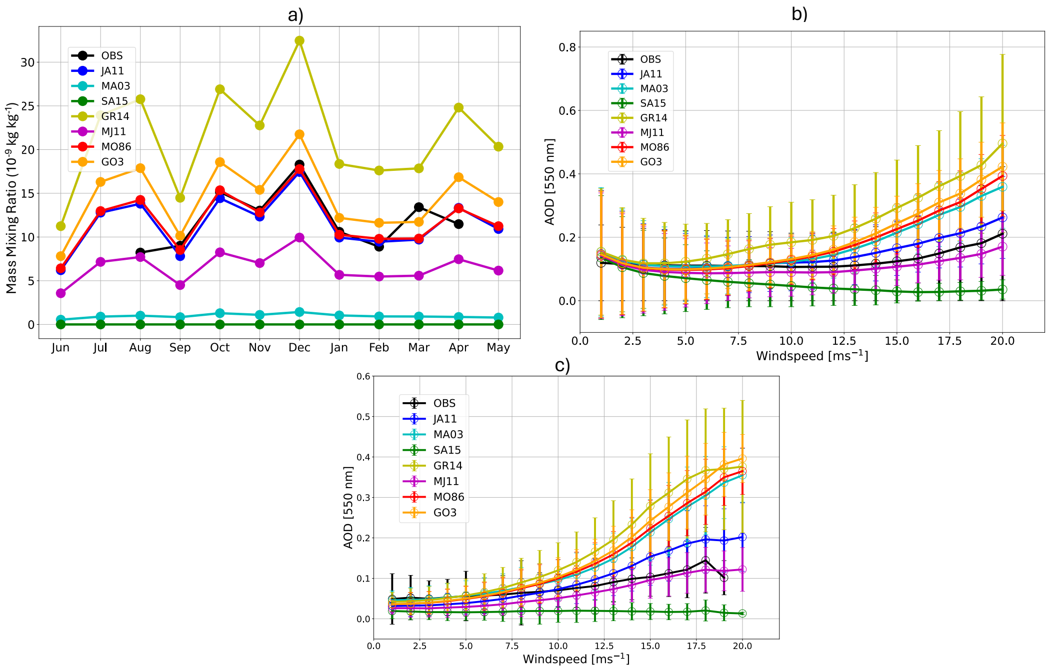

Figure 3: a) Comparison of observations with UKESM1-AMIP sensitivity simulations. (a) Near-surface SSA mixing ratio measured at Cape Grim (40.38°S, 144.4°E) compared to simulations. (b) AOD–wind speed relationship in simulations compared to MODIS AOD and ERA-5 windspeed (global). (c) As for (b) but for the Southern Ocean (40°S-60°S) during austral winter (June, July, August; JJA). Daily averages of AOD were matched to 10 m windspeed for ocean grid cells. These values were then sorted to discretized 1 m s^{-1} bins and the mean AOD in each bin was calculated. Error bars indicate the standard deviation of AOD values present in each of the bin. Cape Grim SSA mixing ratio data are not available for May, June and July. ERA-5 windspeed for JJA over the Southern Ocean doesn't exceed 19 m s^{-1}.

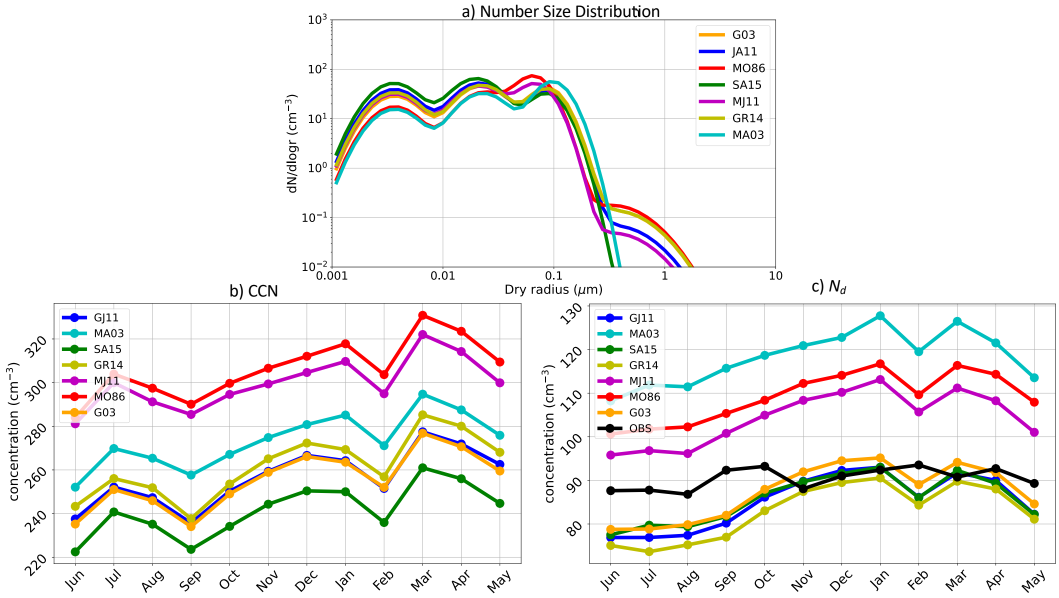

Figure 4: Results from UKESM1-AMIP sensitivity simulations for global-mean (a) Aerosol number size distribution (annual mean), (b) Monthly-mean cloud condensation nuclei concentration at 800 m above the surface (≈ cloud base height), (c) Monthly-mean cloud droplet number concentration (N_d). Note that the G03 result in (a) is visible in the nucleation and Aitken mode, but overlaps GR14 in the accumulation and coarse mode where it is not clearly visible.

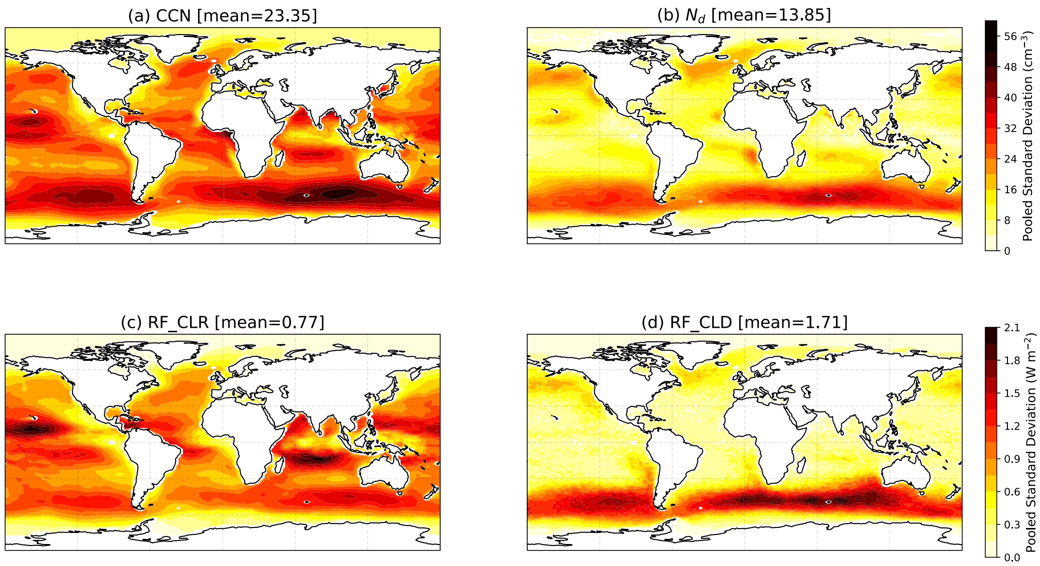

Figure 5: Pooled standard deviation calculated for the UKESM1-AMIP sensitivity simulations: (a) Cloud condensation nuclei (CCN) concentration; (b) N_d concentration; (c) Clear-sky radiative forcing; (d) Cloudy-sky radiative forcing.

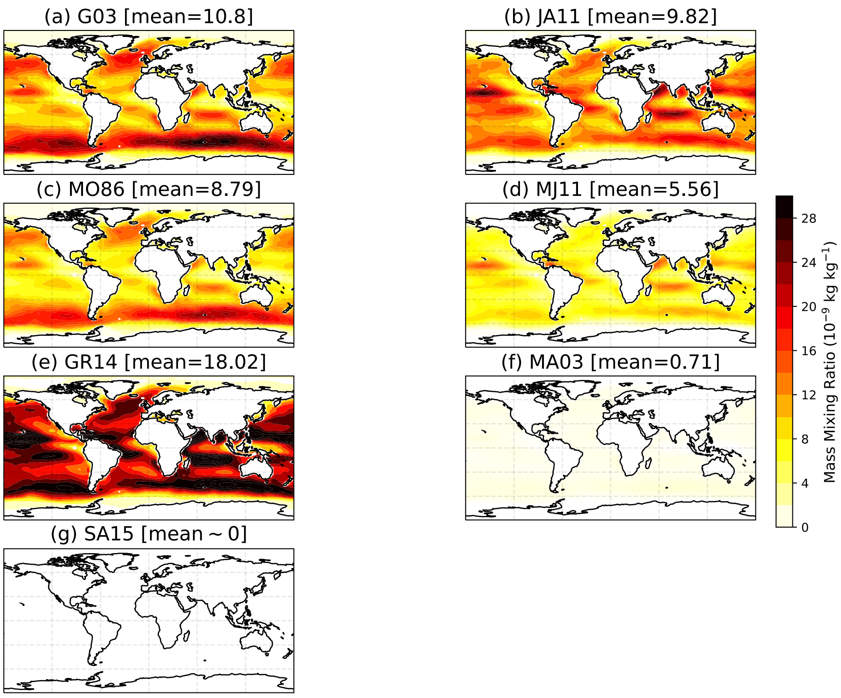

Figure S1: Near surface SSA mass mixing ratio in UKESM1-AMIP simulations with parameterizations of a) G03, b) JA11, c) MO86, d) MJ11, e) GR14, f) MA03, g) SA15. The changes in SSA mass mixing ratio are neglibile when the parameterization of SA15 is implemented in UKESM1. Lower values for the simulation with parameterization with MA03 is likely due to emissions only in accumulation mode. The global mean in each of the simulations are shown within the figure.

Figure_2.pdf.

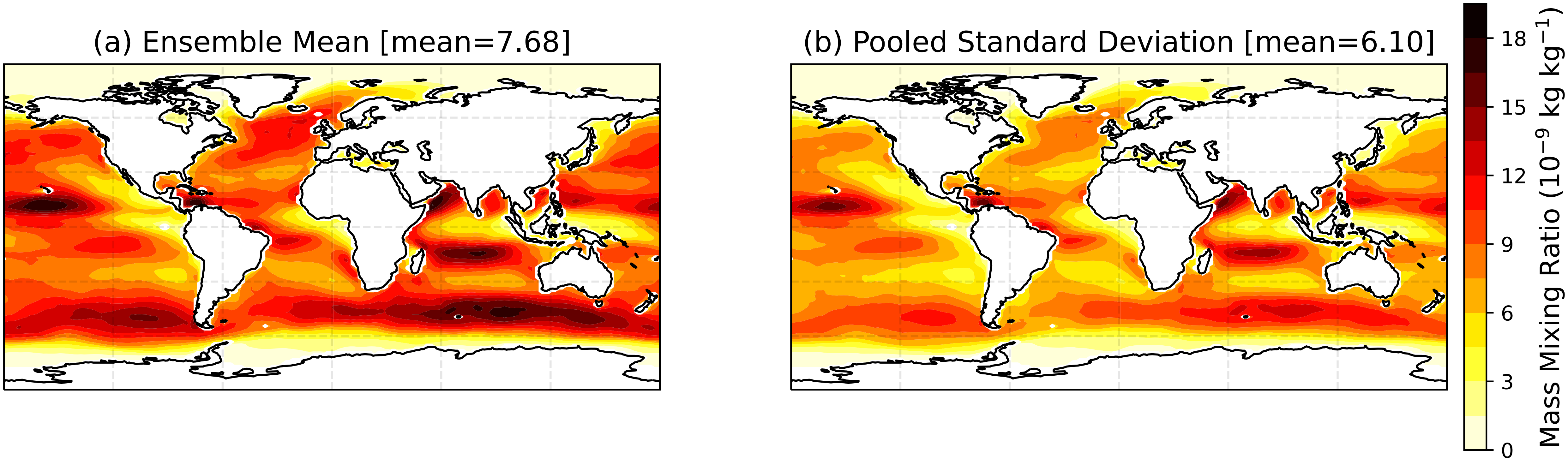
(a) Ensemble Mean [mean=7.68]
(b) Pooled Standard Deviation [mean=6.10]
Mass Mixing Ratio (10^{-9} kg kg^{-1})
0
3
6
9
12
15
18

Figure_1_seconf_version.pdf.

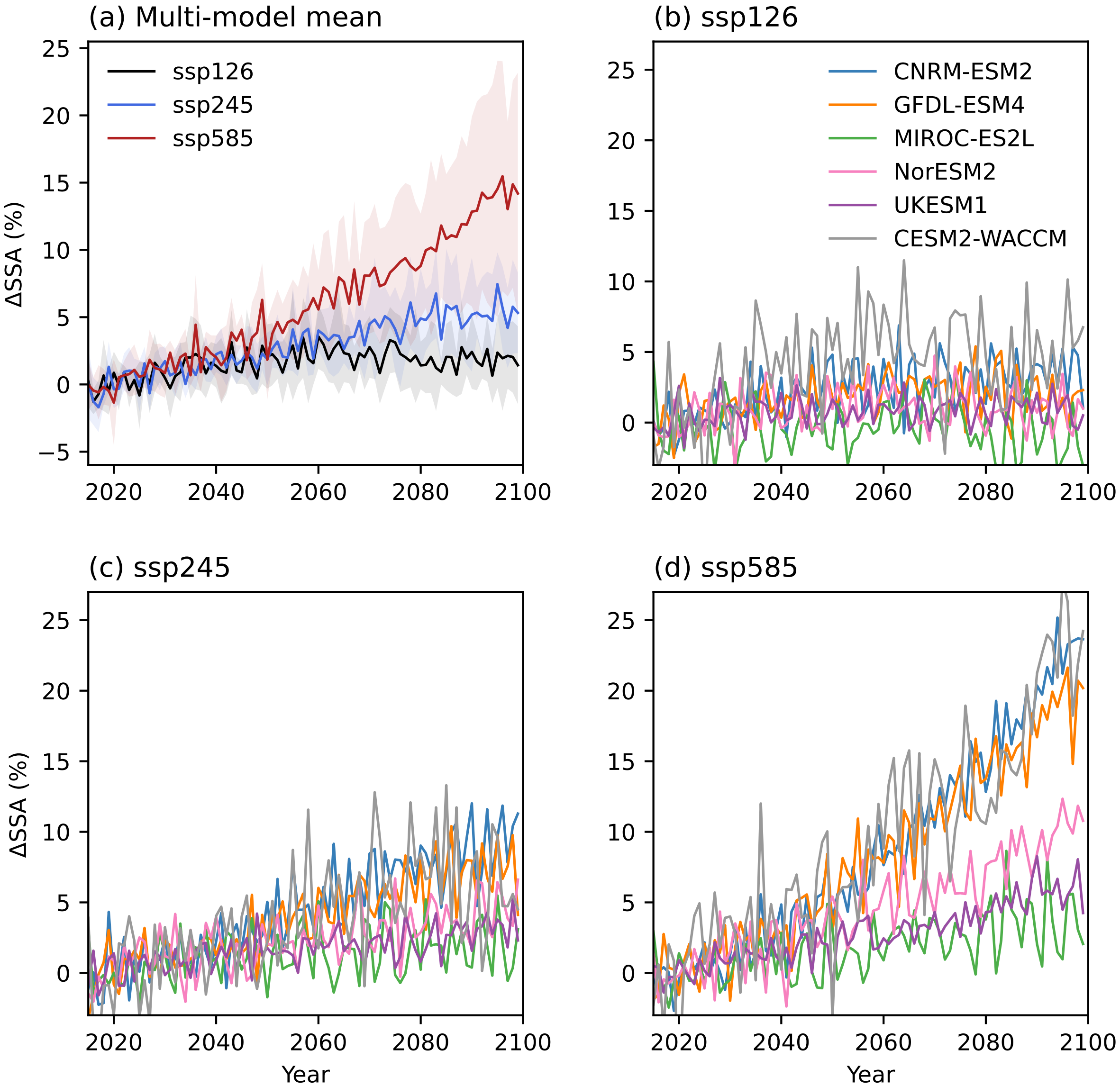
(a) Multi-model mean
(b) ssp126
(c) ssp245
(d) ssp585
ssp126
ssp245
ssp585
CNRM-ESM2
GFDL-ESM4
MIROC-ES2L
NorESM2
UKESM1
CESM2-WACCM
ΔSSA (%)
Year
2020
2040
2060
2080
2100
−5
0
5
10
15
20
25

Fig_4_final_thickline.pdf.

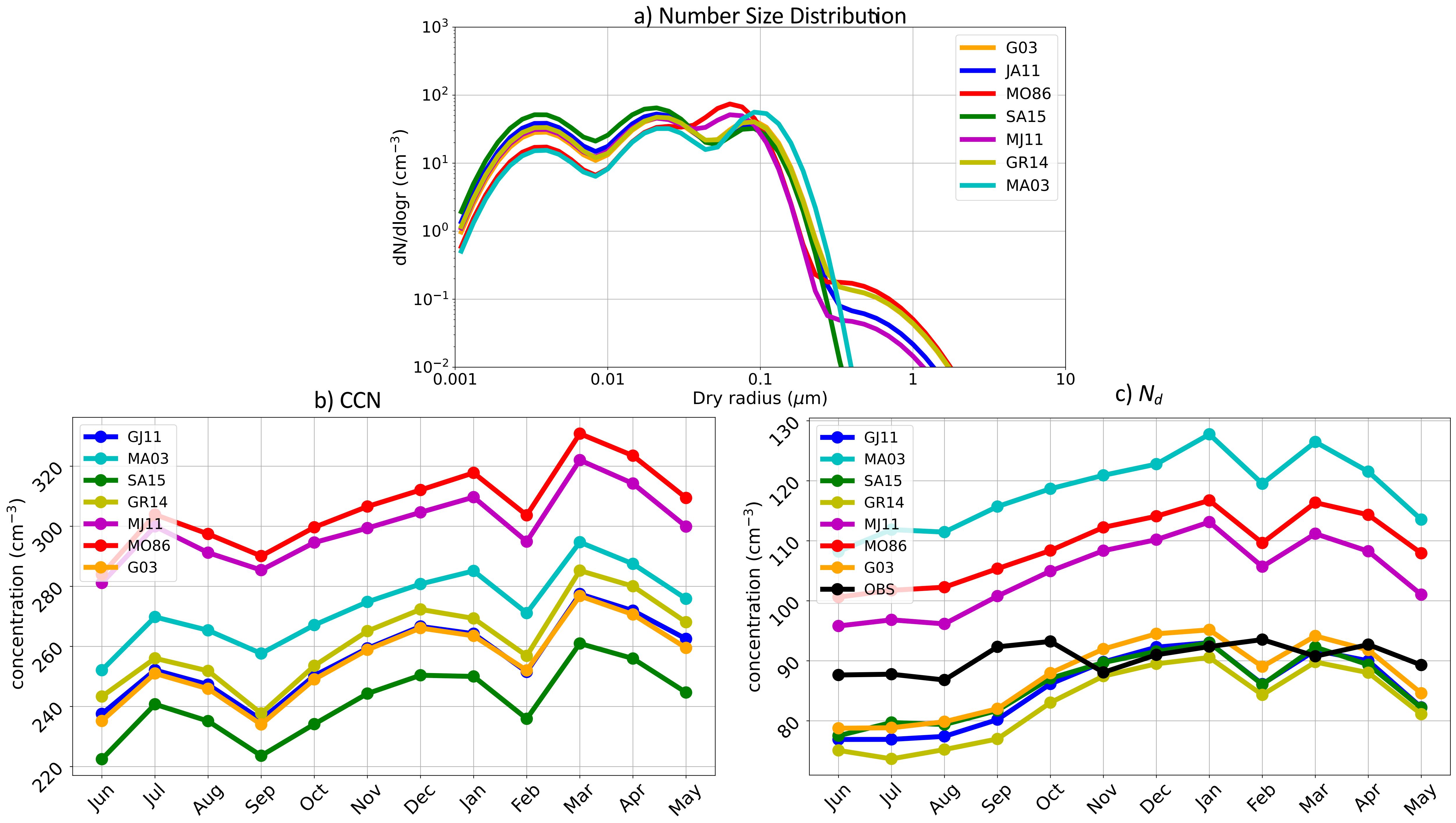
a) Number Size Distribution
dN/dlogr (cm^{-3})
Dry radius (μm)
G03
JA11
MO86
SA15
MJ11
GR14
MA03
b) CCN
concentration (cm^{-3})
GJ11
MA03
SA15
GR14
MJ11
MO86
G03
c) N_d
concentration (cm^{-3})
GJ11
MA03
SA15
GR14
MJ11
MO86
G03
OBS
Jun
Jul
Aug
Sep
Oct
Nov
Dec
Jan
Feb
Mar
Apr
May

Figure_S1.pdf.

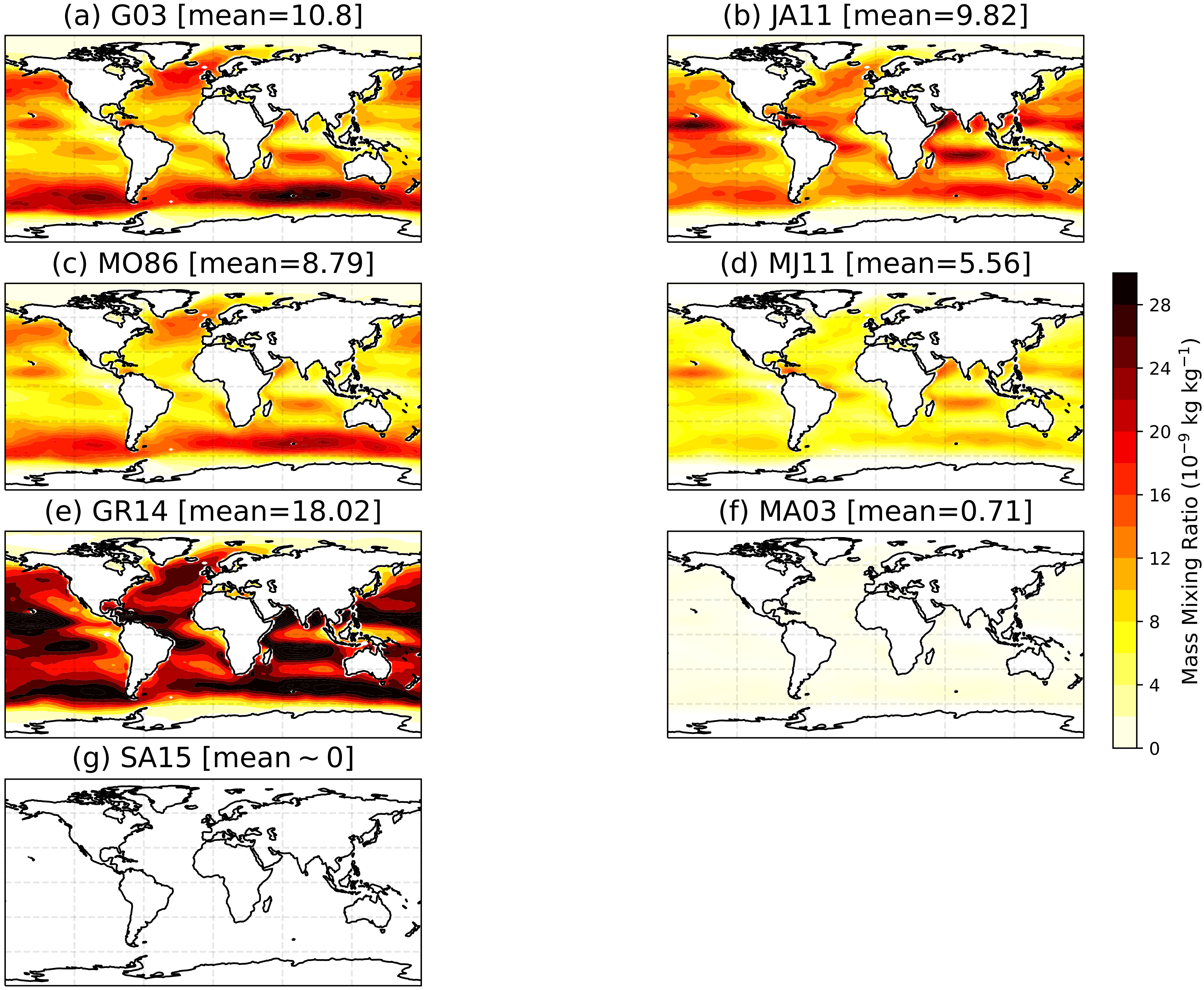
(a) G03 [mean=10.8]
(b) JA11 [mean=9.82]
(c) MO86 [mean=8.79]
(d) MJ11 [mean=5.56]
(e) GR14 [mean=18.02]
(f) MA03 [mean=0.71]
(g) SA15 [mean ~ 0]
Mass Mixing Ratio (10^{-9} kg kg^{-1})
0
4
8
12
16
20
24
28

Figure_3.pdf.

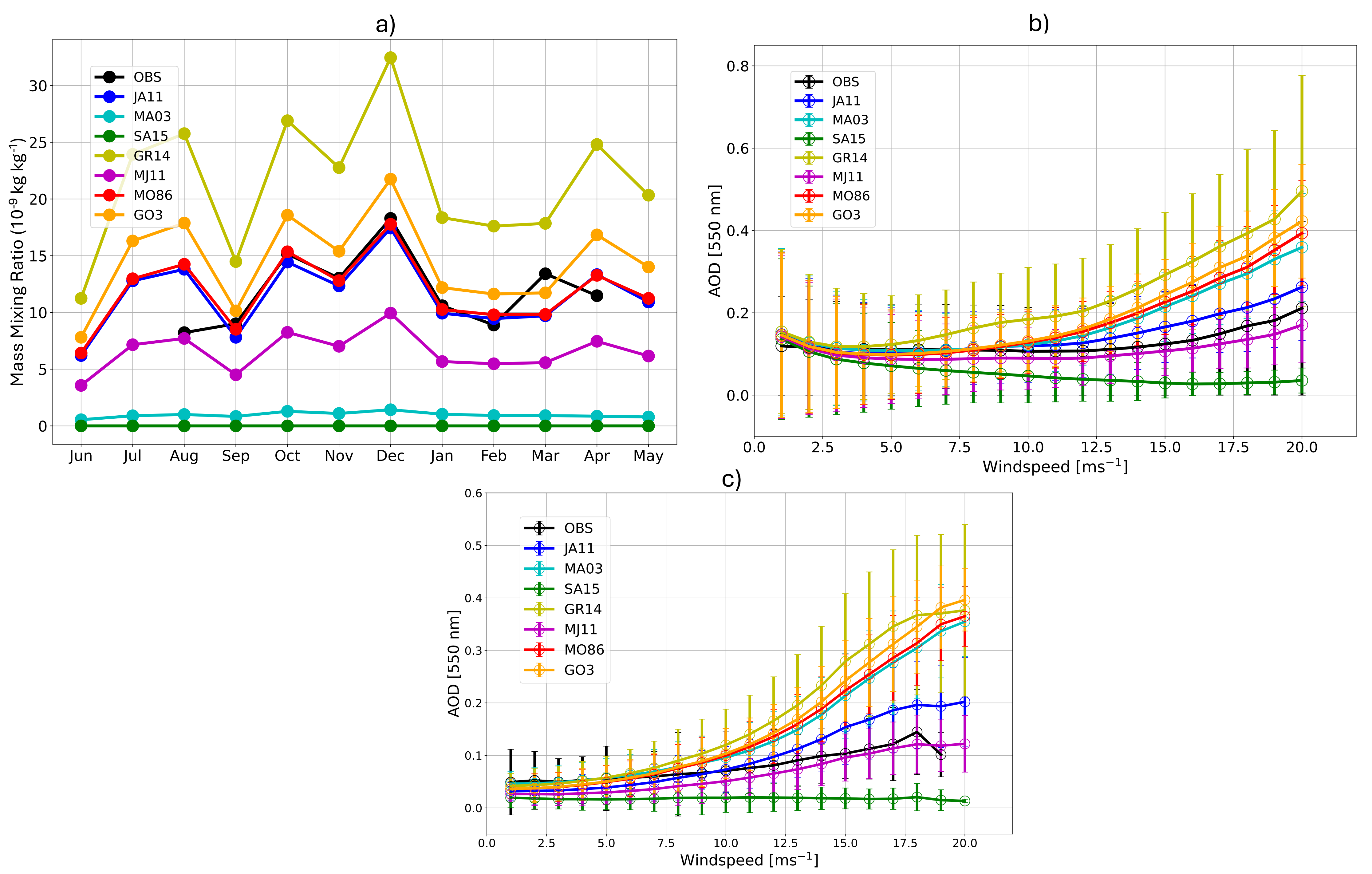

a)
Mass Mixing Ratio (10^{-9} kg kg^{-1})
0
5
10
15
20
25
30
Jun
Jul
Aug
Sep
Oct
Nov
Dec
Jan
Feb
Mar
Apr
May
OBS
JA11
MA03
SA15
GR14
MJ11
MO86
GO3
b)
AOD [550 nm]
0.0
0.2
0.4
0.6
0.8
0.0
2.5
5.0
7.5
10.0
12.5
15.0
17.5
20.0
Windspeed [ms^{-1}]
OBS
JA11
MA03
SA15
GR14
MJ11
MO86
GO3
c)
AOD [550 nm]
0.0
0.1
0.2
0.3
0.4
0.5
0.6
0.0
2.5
5.0
7.5
10.0
12.5
15.0
17.5
20.0
Windspeed [ms^{-1}]
OBS
JA11
MA03
SA15
GR14
MJ11
MO86
GO3